Extension of thickened and hot lithospheres: Inferences from laboratory modeling

Tirel, C.; Brun, J.P.; Sokoutis, D.

published in
Tectonics
2006

DOI (link to publisher)
10.1029/2005TC001804

document version
Publisher's PDF, also known as Version of record

Extension of thickened and hot lithospheres: Inferences from laboratory modeling

C. Tirel,[1,2] J.-P. Brun,[1] and D. Sokoutis[3]

Received 16 February 2005; revised 20 July 2005; accepted 1 November 2005; published 3 February 2006.

[1] The extension of a previously thickened lithosphere is studied through a series of analogue experiments. The models deformed in free and boundary-controlled gravity spreading conditions that simulate the development of wide rift-type and core complex-type structures. In models, the development of structures mainly depends on boundary velocity and therefore on bulk strain rate. Wide rifts are of tilted block-type at high strain rate and of horst- and graben-type at low strain rate. The development of metamorphic core complex-type structures is enhanced by low strain rates and by the presence of weak heterogeneities within the ductile crust. Core complexes result from a necking instability of the upper crust creating a graben, which further widens, allowing the rise and exhumation of a ductile layer dome. An upward convex detachment, flat on top of the dome and steeper on dome limb, appears not to be the primary cause of the core complex development but its consequence. **Citation:** Tirel, C., J.-P. Brun, and D. Sokoutis (2006), Extension of thickened and hot lithospheres: Inferences from laboratory modeling, *Tectonics*, *25*, TC1005, doi:10.1029/2005TC001804.

1. Introduction

[2] Since more than two decades, domains of large-scale lithosphere extension like the Basin and Range of western United States [*Smith and Eaton*, 1978], or the Aegean [*McKenzie*, 1978; *Le Pichon*, 1982] have attracted considerable attention and became the central reference for modeling the mechanical behavior of extending orogenic belts [e.g., *Wernicke*, 1990; *Buck*, 1991; *Royden*, 1996; *McKenzie and Jackson*, 2002]. These domains of so-called "wide rifting" [*Buck*, 1991], take place after a previous stage of crustal thickening [e.g., *Coney and Harms*, 1984] leading to the development of extensional structures as large as 1000 km [*Stewart*, 1978; *Mercier*, 1981]. The identification of metamorphic core complexes, as parts of the ductile crust exhumed at an early stage of the extension [*Davis and Coney*, 1979; *Crittenden et al.*, 1980], constituted a major breakthrough that stimulated numerous attempts to explain their origin [*Wernicke*, 1981, 1985; *Buck*, 1988; *Wernicke and Axen*, 1988; *Buck*, 1991]. Moreover, the flat geometry of the Moho below domains of large-scale extension (Basin and Range [*Allmendinger et al.*, 1987; *Hauser et al.*, 1987] and Aegean [*Makris and Vees*, 1977]) is a fundamental character that identifies wide rifts from narrow rifts. To maintain the Moho flat, despite the variations of stretching amounts in the upper crust, especially in metamorphic core complexes, the middle-lower crust must be able to easily flow laterally. This strongly constrains the thermal state of the lithosphere and rheology at onset of extension [*Block and Royden*, 1990; *Wernicke*, 1990; *Buck*, 1991].

[3] Field studies have largely documented that mountain building is accompanied by temperature rise, metamorphism, partial melting and ductile flow in crustal rocks. Modeling of thermal relaxation, induced by crustal thickening, indicates that Moho temperatures can reach the range 800°–1000°C at depths of 50–60 km some 10 Myr after thickening [*Oxburg and Turcotte*, 1974; *England and Richardson*, 1977; *England and Thompson*, 1986]. In addition, in large mountain belts where thickening is maintained long enough, other phenomena can contribute to the increase of crustal temperatures (e.g., magma emplacement in the middle and lower crust, mantle delamination [*Bird*, 1979] or thermomechanical erosion of the lithospheric mantle by small-scale convection [*Doin and Fleitout*, 1996]). For Moho temperatures higher than 700°C, the strength of the lithosphere is reduced (Figure 1a) to such a degree that gravitational collapse is likely to occur [*Sonder et al.*, 1987; *Gaudemer et al.*, 1988; *Ranalli*, 1997]. Gravitational collapse and related crustal extension [*Rey et al.*, 2001] occurs in most orogens of alpine age [*Dewey*, 1988] as well as in older phanerozoic ones (e.g., Hercynian [*Burg et al.*, 1994] and Caledonian [*Andersen et al.*, 1991]). For the above reasons, the domains of large-scale extension (Figure 1b) can be considered to result from the gravity spreading of a hot and weak lithosphere. However, gravity spreading of the whole lithosphere necessarily depends on the displacement rate of plates that surrounds an unstable orogenic domain. In other words, the extension of a previously thickened lithosphere is controlled by plate kinematics at its boundaries.

[4] The present paper examines the modes of extension of a thickened and weak brittle-ductile lithosphere using analogue model experiments. The models only represent the crustal part of the lithosphere by having the lower boundary condition of free slip at model base that simulates the

[1]Géosciences Rennes, Université de Rennes 1, UMR 6118, Rennes, France.
[2]Now at Faculty of Geosciences, Tectonophysics, Utrecht University, Utrecht, Netherlands.
[3]Netherlands Centre for Integrated Solid Earth Science, Faculty of Earth and Life Sciences, Vrije Universiteit, Amsterdam, Netherlands.

0278-7407/06/2005TC001804$12.00

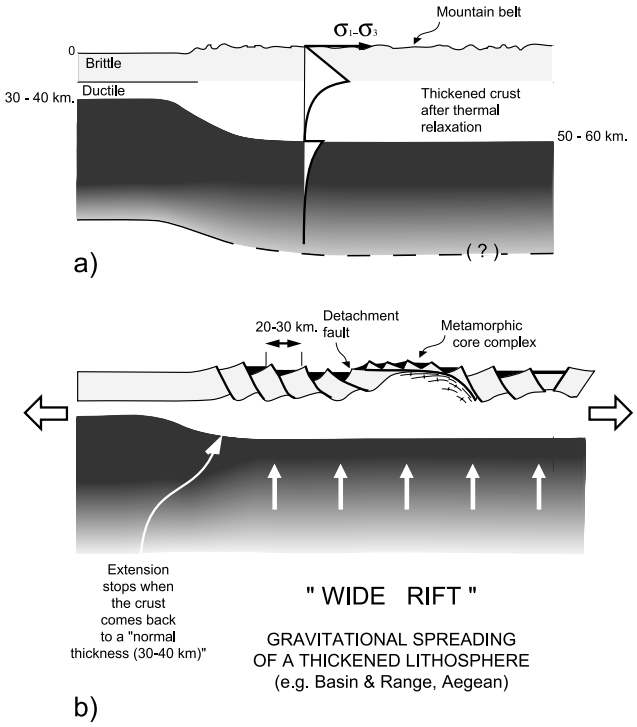

Figure 1. Model of gravitational spreading of a thickened and thermally relaxed lithosphere (modified after *Brun* [1999]). (a) Initial condition. (b) Ongoing extensional stage.

presence of a virtual mantle, extending at the same rate than the crust. Two types of experiment are carried out, namely, free gravity spreading and boundary-controlled gravity spreading, the former used to calibrate the latter. The results show the effect of boundary velocity on the dynamics of extension and resulting deformation patterns. The discussion concerns the development of wide rift versus metamorphic core complexes, the dynamics of faulting in the upper brittle crust and the origin and development of metamorphic core complexes.

2. Experimental Procedure

[5] The analogue experiments intend to simulate the extension of a two-layer brittle-ductile system made of dry feldspar sand and silicone putty of Newtonian behavior that represent the upper brittle and the lower ductile crust of a thickened lithosphere, respectively. The models are made of 4.5 cm of sand lying on top of 9.0 cm of silicone putty, which would correspond in nature to a 20 km deep brittle-ductile transition within a 60 km thick crust. The basal boundary of models rests on top of a lubricated rigid plate to take into account the flat Moho geometry observed in nature below metamorphic core complexes and wide rift areas. Basal lubrication is made using liquid soap whose viscosity is in the order of 1 Pa s that is to say 4 orders of magnitude lower than model silicone putty. This is basically the same procedure of modeling previously used by *Brun et al.* [1994]. This experimental boundary condition implies that the crust and the underlying mantle undergo the same bulk amount of stretching.

[6] The models, whose initial dimensions are LHW = 30 × 13.5 × 13 cm, are built in a rectangular box (60 × 15 × 15 cm) in size (Figure 2). One of the vertical extremities of the model, a mobile wall can displace under the horizontal pressure of the model, i.e., gravity spreading, or is pulled at constant rate by a screw jack controlled by a stepping motor. The lateral sides of the silicone layer are lubricated to reduce the lateral boundary shear effects.

2.1. Materials

[7] The feldspar sand behaves as a Mohr-Coulomb material with a 30° friction angle and 1.18 g cm^{-3} density. Two different types of silicone putty with Newtonian behavior have been used to model ductile lower crust and a local weakness anomaly (Figure 2). The ''lower crust'' silicone putty has a 1.4 g cm^{-3} density and a 10^4 Pa s viscosity at controlled room temperature (25°C ± 1) (for more details, see *Nalpas and Brun* [1993]). The ''anomalous'' silicone putty has a 1 g cm^{-3} density and a 0.6 × 10^3 Pa s viscosity. It has already been shown by *Brun et al.* [1994] that brittle-ductile two-layer models that do not involve a viscosity anomaly stretch almost homogeneously giving titled blocks in the sand layer. This type of models gives a wide rift-type mode of extension [*Brun*, 1999]. Core complex-type structures are only obtained in models containing an anomaly located below the sand-silicone interface. This has led *Brun* [1999] to propose that core complexes could be considered as likely representing an anomaly within the wide rift mode of *Buck* [1991]. It is noteworthy that the same type of dual behavior of models, with and without a viscosity-density anomaly, also prevails in numerical modeling of core complexes [*Tirel et al.*, 2004]. In geological terms, such anomalies may correspond to partially molten zones or hot granite intrusions, which are commonly observed in metamorphic core complexes.

2.2. Scaling

[8] For a small-scale model to be representative of a natural example (a prototype), a dynamic similarity in terms

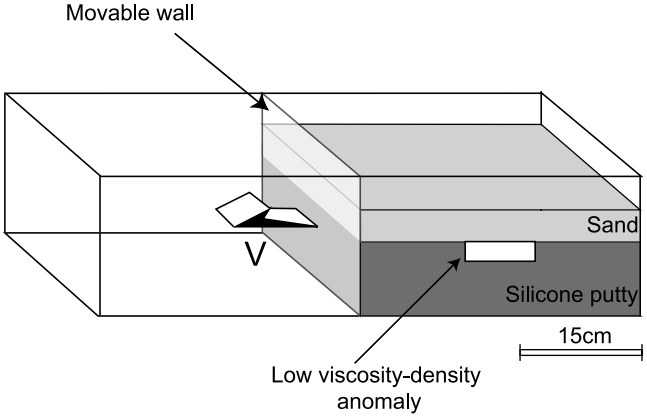

Figure 2. Experimental setup. The viscosity-density anomaly is present in only some of the models.

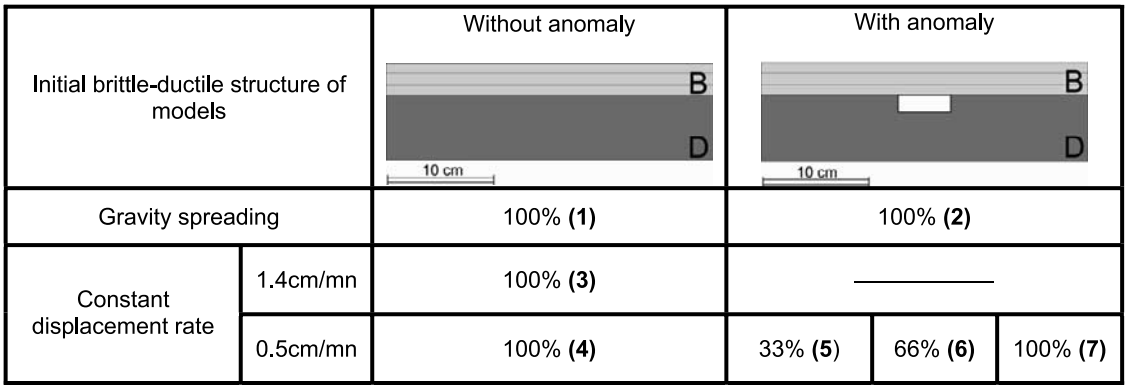

Figure 3. Input parameters of the experiments. Numbers indicate the percentage of bulk horizontal stretching. Model numbers are in parentheses.

of distribution of stresses, rheologies and densities between the model and the prototype is required [*Hubbert*, 1937; *Ramberg*, 1981]. The basic principle of the method consists of simulating simplified strength profiles, which incorporate brittle (frictional) and ductile (viscous) rheologies with gravity forces. Scaling relationships between the prototype and the model are obtained by keeping the average strength of the ductile layers correctly scaled with respect to the strength of the brittle layers and the gravity forces.

[9] It can be shown, from the equation of dynamics, which in experiments made under natural gravity:

$$\sigma^* = \rho^* g^* L^*, \tag{1}$$

where $\sigma^* = (\sigma_m/\sigma_n)$, $\rho^* = (\rho_m/\rho_n)$, $g^* = (g_m/g_n)$ and $L^* = (L_m/L_n)$ are model (m) to nature (n) ratios of stress (σ^*), density (ρ^*), gravity (g*) and length (L*). The present models being processed under natural gravity $g^* = 1$. Model and nature densities being of the same order of magnitude, the density ratio is $\rho^* \approx 1$. Therefore the condition simplifies to [*Brun*, 1999]

$$\sigma^* \approx L^*. \tag{2}$$

For a thickened continental crust of 60 km represented by 13.5 cm thick model, the length ratio is about 10^{-6}. It is accordingly verified that the stress ratio is 10^{-6}.

[10] If we simplify the ductile power law creep equation to Newtonian flow,

$$\dot{\varepsilon}^* = \sigma^*/\eta^*, \tag{3}$$

where $\dot{\varepsilon}^* = (\dot{\varepsilon}_m/\dot{\varepsilon}_n)$ and $\eta^* = (\eta_m/\eta_n)$ are the scaling ratios for strain rate and viscosity, respectively. In term of bulk strain at the model scale, this gives

$$\dot{\varepsilon}^* = V^*/L^*, \tag{4}$$

where $V^* = (V_m/V_n)$ is the scaling ratios of velocity. From the above equations, the brittle-ductile strength ratio in models can be calculated. As an example, in experiment carried out at a velocity of 0.5 cm min^{-1} the brittle-ductile strength ratio is equal to 40. Taking a brittle strength of around 500 MPa close the brittle-ductile transition in nature [*Byerlee*, 1978] a ratio of 40 predicts a mean viscosity of 10^{19} Pa s for the ductile crust, close to the one found by Clark and Royden [*Clark and Royden*, 2000] for the ductile crust of Tibet.

2.3. Experiments

[11] The experiments were performed at the Tectonic Laboratory of the Vrije Universiteit Amsterdam (Netherlands). The parameters of the seven experiments presented here are summarized in Figure 3. Two of them were of gravity spreading type (models 1 and 2) and five were run at constant extension rate of 1.4 cm min^{-1} (model 3) and 0.5 cm min^{-1} (models 4 to 7). The above values have been chosen because of the strain rate dependence of the silicone layer strengths. Such a range of displacement rates allows exploring the effects of variations in ductile strength through 1 order of magnitude, keeping the brittle strength constant. In gravity spreading-type experiments the velocity of the mobile wall decreases exponentially during extension (Figure 4). This may correspond in nature to a thickened lithosphere extending under its own weight without any boundary limitation. However, in nature, domains of thickened lithosphere would be able to extend as a function of surrounding plate divergence. As an example of this, the Aegean extension is a consequence of the retreat of the south Hellenic subducting slab [*Le Pichon*, 1982; *McClusky et al.*, 2000]. Therefore we calibrated the constant extension rates of 1.4 and 0.5 cm min^{-1} on the basis of velocities observed in gravity spreading experiments (Figure 4a). Bulk stretching increases linearly with time in experiments with constant rate whereas it is strongly nonlinear in gravity spreading (Figure 4b).

[12] Gravity spreading and constant extension rate models were run with (models 2, 5, 6, and 7) and without (models 1, 3, and 4) a central viscosity-density anomaly located below the brittle-ductile interface. Constant extension rate of 0.5 cm min^{-1} has been used for three experiments at 33, 66, and 100% of bulk stretching (models 5 to

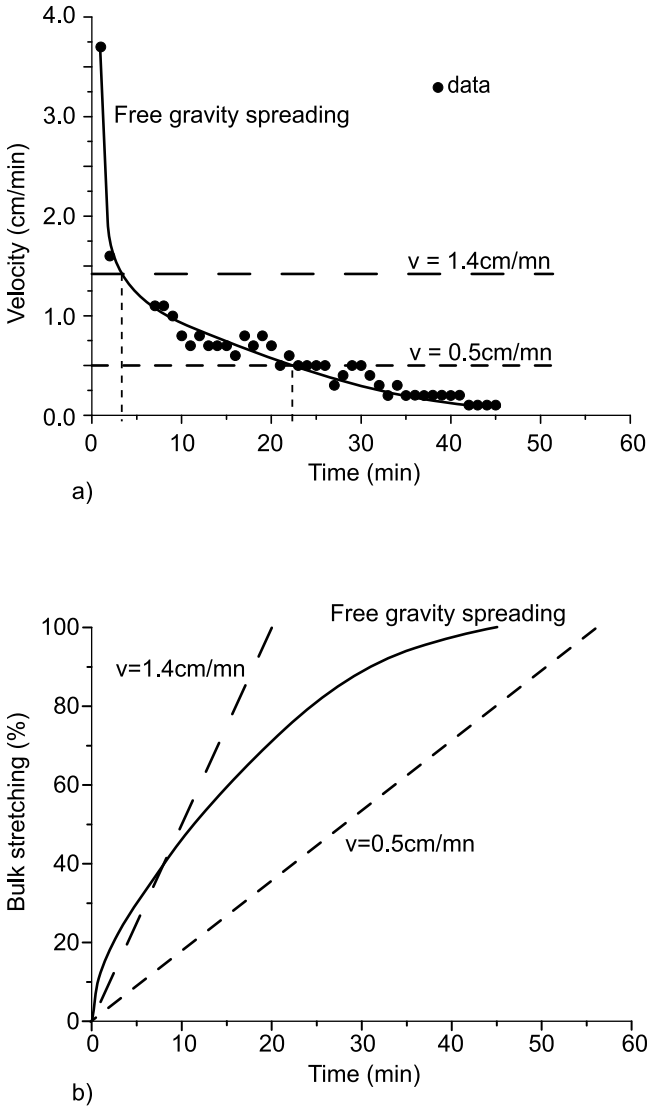

Figure 4. (a) Variation of boundary velocity as a function of time in free gravity spreading models (models 1 and 2). Dots represent the mobile wall velocity measured at regular time intervals during the experiment from surface photographs. Constant boundary velocities of 1.4 and 0.5 cm min^{-1} are those used for models 3 to 7. (b) Variation of bulk model stretching as a function of time in free gravity spreading (models 1 and 2) and in boundary-controlled gravity spreading (1.4 cm min^{-1} for model 3 and 0.5 cm min^{-1} for models 4 to 7).

7) in order to examine the progressive development of a core complex. With the exception of models 5 and 6, all the rest have been deformed up to 100% bulk stretching.

[13] During deformation, the models photographed from above at regular time intervals to facilitate fault development at the upper brittle layer. At the end, the models were soaked in the water, frozen, and cut into longitudinal strips to expose cross sections for photographs of the internal structures. Cross sections presented in the paper correspond to those cut at model middle axis, such as to avoid any strong boundary effect.

3. Free Gravity Spreading Models

3.1. Model 1, Without Anomaly

[14] This model displays an almost regular pattern of parallel faults dipping toward the fixed vertical end wall (Figure 5). Most of the faults developed at an early stage of deformation and accommodated further stretching by rotation. As argued in previous works, the normal fault sense of dip is likely controlled by the sense of shear at the brittle-ductile interface [*Faugère and Brun*, 1984; *Vendeville et al.*, 1987; *Brun*, 1999]. However, some secondary normal faults with limited offset (see thin lines on Figure 5) were created during block tilting. Along most of the section, the envelope of (1) the interface between the brittle and ductile layers and (2) the top surface of the brittle layer remain nearly horizontal. The only discrepancy occurs close to the moving wall.

3.2. Model 2, With a Viscosity-Density Anomaly

[15] When a density-viscosity anomaly is placed below the brittle-ductile interface, at the center of the model, the deformation pattern changes drastically (Figure 6). A dome develops at the central part of the model, being directly related to the ductile anomaly. To the dome's right, the brittle layer is affected by left dipping normal faults defining large tilted blocks that demonstrate an increase of stretching toward the dome. At the left side of the dome, the brittle layer is more faulted and thinned. The fault pattern combines conjugate faults and parallel faults, defining narrow tilted blocks.

4. Boundary-Controlled Gravity Spreading Models

[16] Models with initial conditions, i.e., materials and geometry, similar to those of models 1 and 2 were deformed at two different constant displacement rates of the moving end wall, calibrated by reference to the velocity curve of gravity spreading models (see Figure 4a). Two velocities of 1.4 and 0.5 cm min^{-1} were chosen to match (1) the end of steep part and (2) the middle of the low-dipping part of the velocity curve, respectively.

4.1. Model 3, v = 1.4 cm min^{-1} Without Anomaly

[17] The model (Figure 7a) displays a strong structural asymmetry due to the juxtaposition of three domains that are from right to left: (1) a domain of conjugate and right dipping normal faults that accommodate a moderate thinning of the brittle layer, (2) a domain of left dipping parallel faults defining narrow tilted blocks that accommodate a stronger thinning of the brittle layer, and (3) a domain of collapse close to the moving end wall.

[18] This lateral partitioning in three domains of contrasted deformation is a direct consequence of the imposed extension rate and cumulative amounts of bulk model stretching at progressive stages of deformation. The curves

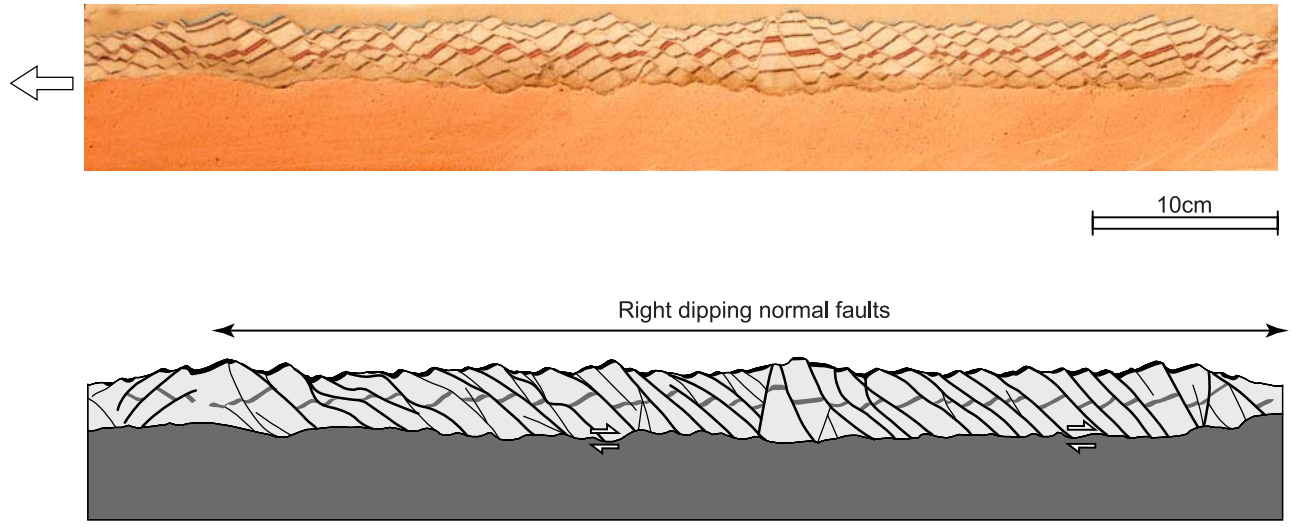

Figure 5. Cross section of model 1 in free gravity spreading without anomaly. Open arrows indicate the sense of shear at the brittle-ductile interface.

shown in Figure 4b intersect at around 40% of progressive bulk model stretching. After this critical value, the ductile layer had not the possibility to flow fast enough to accommodate the bulk stretching of 100% and therefore to maintain horizontal at once the brittle-ductile interface and the surface of the brittle layer. Stretching then progressively localized in the left half part of the model, a process that ended up with the collapse of the left extremity, close to the moving wall.

[19] The senses of shear at the brittle-ductile interface, as deduced from domains of block tilting, are opposite, top to the right and top to the left, at the right and left parts of the model, respectively. This indicates that the strain rate was lower or equal to that of gravity spreading, away from the moving wall. On the contrary, closer to the moving wall, the strain rate became higher than that of gravity spreading. The difference in ductile layer thickness between the right and left parts of the model indicates a lateral flow of ductile material from right to left, likely in the second part of the deformation when the critical value of 40% bulk stretching has been passed.

4.2. Model 4, v = 0.5 cm min^{-1} Without Anomaly

[20] The model shows two main types of structural domains in the brittle layer (Figure 7b): (1) domains of moderate stretching with conjugate normal faults defining

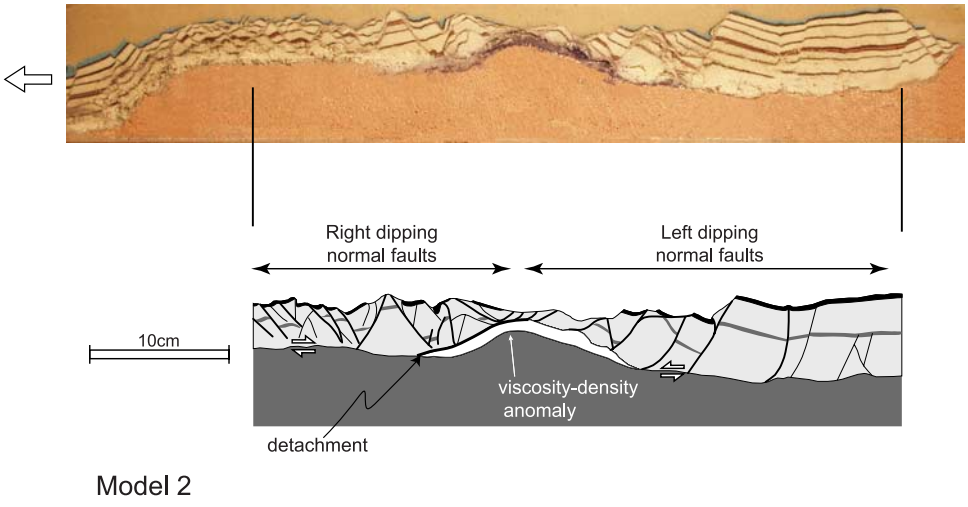

Figure 6. Cross section of model 2 in free gravity spreading with a low viscosity-density anomaly in the ductile layer. The line drawing does not take into account the boundary effects. Open arrows indicate the sense of shear at the brittle-ductile interface.

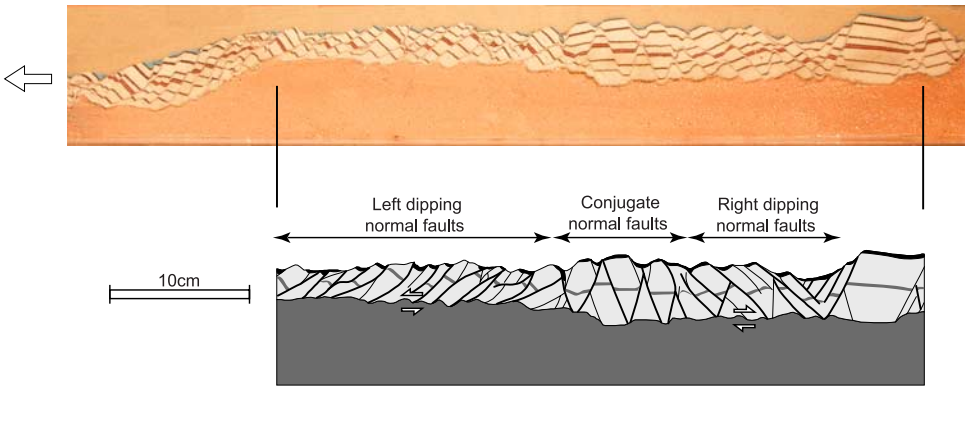

Figure 7. Cross sections of models 3 and 4 in boundary-controlled gravity spreading without anomaly in the ductile layer. Constant boundary velocities are of (a) 1.4 cm min^{-1} for model 3 and (b) 0.5 cm min^{-1} for model 4. The line drawings do not take into account the boundary effects. Open arrows indicate the sense of shear at the brittle-ductile interface.

horst and graben structures with some tilted blocks and (2) domains of intense stretching and layer thinning. Besides the domal rise of the ductile layer, which is localized below the zones of intense stretching, the envelope of the brittle-ductile interface remained horizontal.

[21] This arrangement of structures results from a rather homogeneous conjugate faulting, followed by a necking-type localization within two grabens. The necking zones are defined by symmetrical patterns of narrow spaced and low-dipping normal faults. For comparison with the next models, it is important to note that this necking of the brittle layer did not developed at an early stage but progressively during the experimental deformation (see Appendix A and Figure A1).

[22] The ductile layer is homogeneously thinned, except below the zones of brittle layer necking. In this model where the extension rate is significantly lower than in gravity spreading models, during half of the experimental duration (Figure 4a), the ductile layer is able to flow laterally to compensate lateral variations of stretching in the brittle layer and consequent topographic irregularities. As a whole, the structure of the model is close to symmetrical.

4.3. Models 5, 6 and 7, v = 0.5 cm min^{-1} With Anomaly

[23] These three models (Figure 8) are identical in terms of initial and boundary conditions. They only differ in terms of bulk amounts of stretching. Apart from the viscosity-density anomaly placed below the brittle-ductile interface, at the center of the model, they are directly comparable to model 4. At 33% of bulk stretching, the brittle layer displays a symmetrical graben that developed above the anomaly within the ductile layer and a zone of faulting and block tilting close to the end of the moving wall. Models run-up to 66 and 100% of bulk stretching show basically the same structural features, attesting for the reproducibility of experiments.

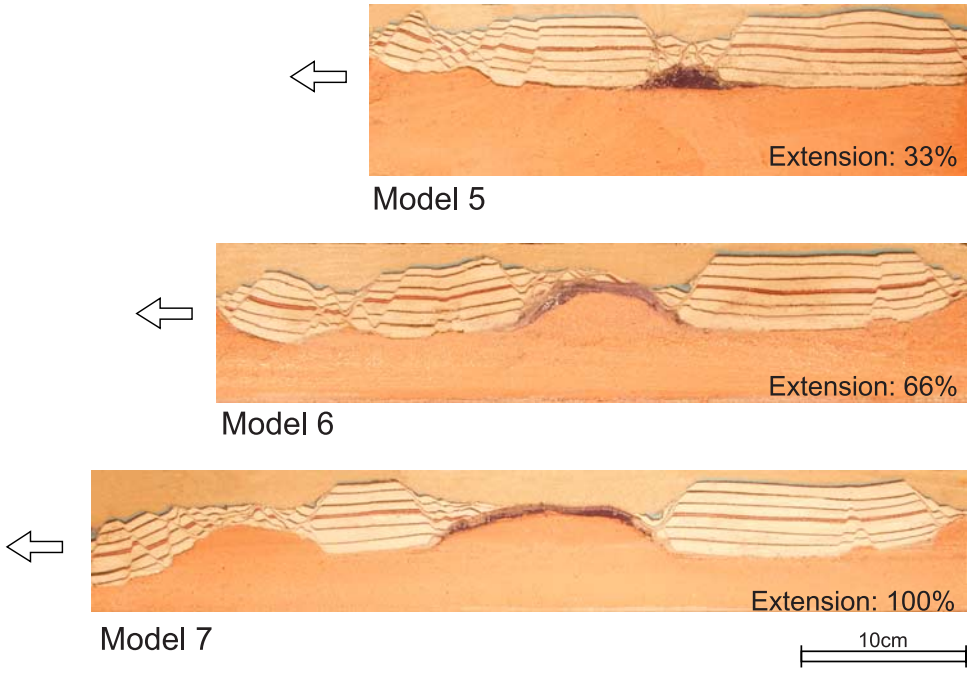

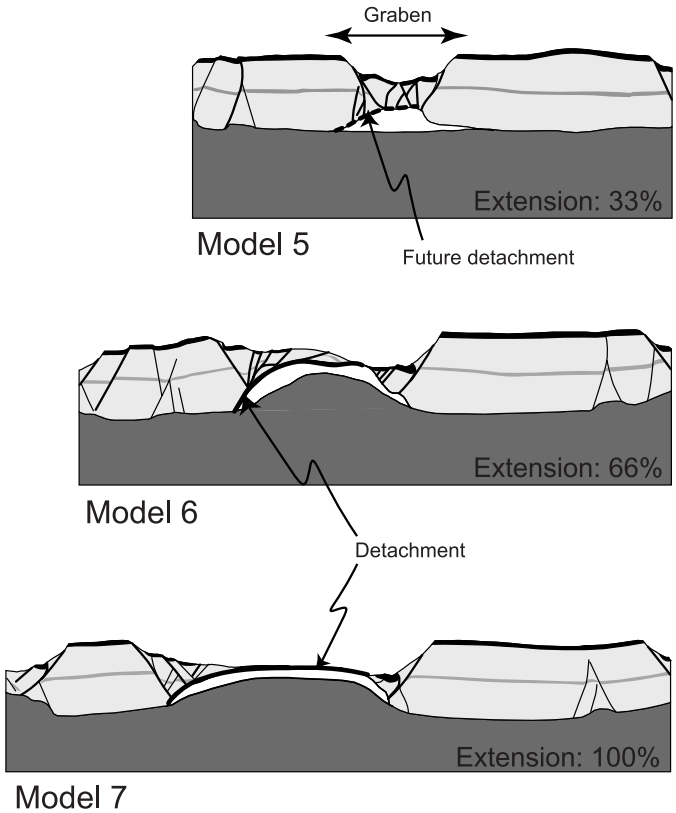

Figure 8. Cross sections of models 5 to 7 showing three stages of core complex development in boundary-controlled gravity spreading with a viscosity-density anomaly in the ductile layer. From top to base the bulk model stretching is 33%, 66%, and 100%. The line drawings do not take into account the boundary effects.

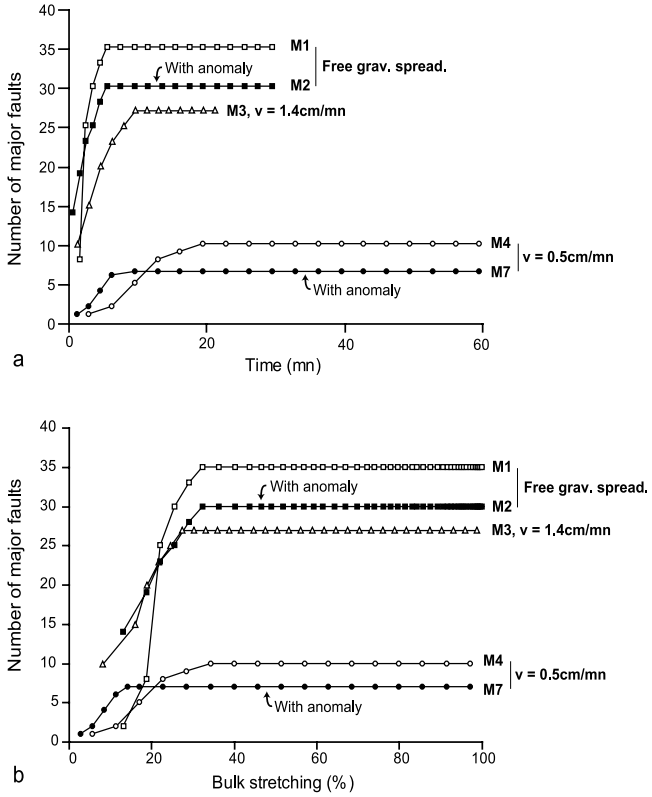

Figure 9. Number of major faults as a function of (a) time and (b) bulk stretching in all presented models.

[24] The evolution of the central graben, at increasing amount of stretching, shows that it becomes the site of a domal rise of the ductile layer by extreme thinning and rupture of the inner part of the graben. Small tilted blocks resulting from that extreme thinning define the hanging wall of a detachment, on the left limb of the dome. The final asymmetrical structure can be directly compared to core complexes.

[25] Like in model 2, the bulk model structure is asymmetrical. To the right of the dome the brittle layer remained almost undeformed. To the left, close to the end of the moving wall, the brittle layer underwent a strong stretching, accommodated by conjugate normal faults and few tilted blocks.

[26] These models show that the presence of an anomaly in the ductile layer is responsible for strain localization at an early stage of deformation. This is at variance with model 4 where localization was a continuous and progressive process during stretching and where the domal rise is accommodated by a symmetrical pattern of faulting.

5. Faulting as a Function of Time and Finite Bulk Stretching

[27] In all models described above, major faults are created during the early stages of extension. This is illustrated in diagrams where the number of major faults is plotted as a function of time (Figure 9a) and bulk stretching (Figure 9b). Measurements of fault pattern development presented in Figure 9 have been carried out on surface photographs taken at regular time intervals during experiment (see Appendix A).

[28] The number of major faults appears to be a direct function of displacement rate. This is exemplified by boundary-controlled gravity spreading models. At 0.5 cm min^{-1} the number of major faults does not pass 10 whereas at 1.4 cm min^{-1} it reaches 27. In free gravity spreading models, where the displacement rate is initially close to 4.0 cm min^{-1} (Figure 4a), the number of major faults reaches 35. In terms of bulk stretching (Figure 9b) the initiation of the whole fault patterns occurs between 15 and 35% at 0.5 cm min^{-1}, at 28% at 1.4 cm min^{-1} and 32 in free gravity spreading models.

[29] The presence of an anomaly within the ductile layer reduces the number of major faults. This is illustrated by boundary-controlled gravity spreading models at 0.5 cm min^{-1} as well as free gravity spreading models. In terms of duration of major fault creation (Figure 9a), free gravity spreading models do not show any significant difference contrary to boundary-controlled gravity spreading models at 0.5 cm min^{-1} (9 min with an anomaly and 20 min without). This difference is also striking in terms of bulk stretching (Figure 9b). All major faults have been created at around 15% of bulk stretching with an anomaly and at 35% without an anomaly. The above results show that the presence of an anomaly drastically changes the faulting dynamics (number of major faults and duration of major fault creation), all the more so since the displacement rate is low.

6. Discussion

[30] The experimental setting took into account the geological and geophysical data available for the Basin and Range (BR) and the Aegean (BR from *Smith and Eaton* [1978], *Allmendinger et al.* [1987], and *Hauser et al.* [1987] and Aegean from *Makris and Vees* [1977], *McKenzie* [1978], and *Le Pichon* [1982]), as well as previous results of numerical modeling [*Sonder et al.*, 1987; *Buck*, 1991]. The upper crustal thickness was therefore fixed in the order of one third of the total crustal thickness before extension, which should represent a 50–60 km thick crust in nature while the bulk amount of stretching reached the 100%. The models that only represent the crustal part of the lithosphere assume that the viscosity contrast between the ductile crust and the sub-Moho mantle is low enough to maintain the Moho close to horizontal during extension. This condition is represented in the experiments by free basal slip of the model above a horizontal rigid plate, simulating a virtual stretching of the lithospheric mantle equal to the bulk crustal model stretching. In terms of boundary displacements, the models belong to two main categories: free gravity spreading and boundary-controlled gravity spreading.

[31] The modeling results bring new insights for the understanding of extension in thickened and "hot" lithospheres. The wide range of observed deformation patterns is relevant to wide rift-type (Figures 10a and 10c) and core

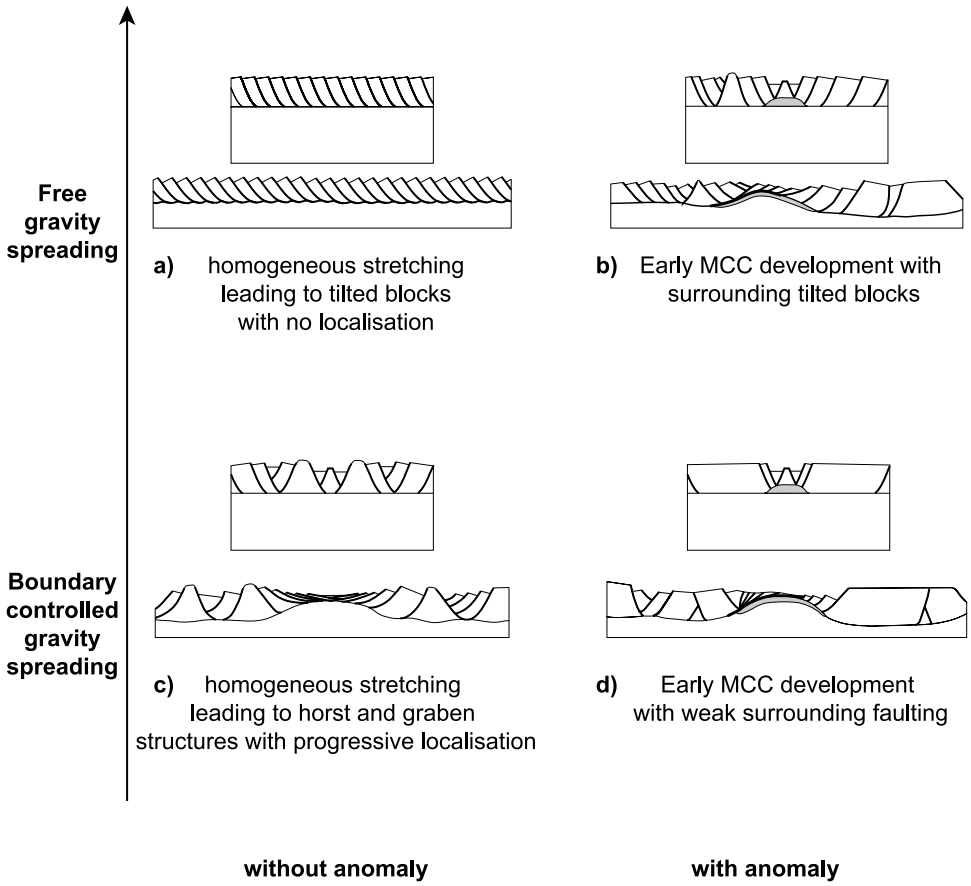

Figure 10. Diagram summarizing the main features of deformation in models according to the boundary velocity (free or controlled gravity spreading) and the presence or absence of anomaly within the ductile layer. MCC, metamorphic core complex.

complex-type (Figures 10b and 10d) modes of extension. Similarities and differences between the models are directly dependant on the input parameters of models, namely, the boundary velocity and the presence or absence of ductile layer heterogeneity.

6.1. Wide Rift Versus MCC

[32] The present results show that the fault patterns, which are relevant to wide rift-type extension (Figures 10a and 10c), are strongly dependant on the boundary velocity and therefore to strain rate and coupling between brittle and ductile layers (B/D coupling; see discussion by *Brun* [1999]). At the highest possible extension rate (i.e., free gravity spreading; Figure 10a), B/D coupling is maximum, leading to the development of large domains of tilted blocks. At lower values of extension rate (i.e., boundary-controlled gravity spreading; Figure 10c), B/D coupling is reduced, favoring conjugate fault patterns and the development of horst and graben-type structures. This confirms previous conclusions gained from analogue modeling [see *Brun*, 1999, Figure 4]. However, it must be noted that a localization effect, which has not been observed previously, occurred at the lower extension rate used (Figure 10c). The brittle layer underwent local symmetrical necking in some of the early grabens accompanied by a domal rise of the ductile layer. This type of structures could possibly be interpreted as core complexes.

[33] Structures more directly comparable to core complexes were obtained in models that involved a density-viscosity anomaly located below the brittle-ductile interface (Figures 10b and 10d). In free gravity spreading, the model structure (Figure 10b) is similar to that of *Brun et al.* [1994]. In experiments with boundary controlled velocity (Figure 10d) the models display a strong and early localization effect that is not observed in free gravity spreading. This is in good agreement with the well-established fact of the early development of core complexes in the natural systems (Basin and Range from *Coney* [1987] and Aegean from *Gautier et al.* [1999]). It is therefore somewhat puzzling to consider from model evidence (Figure 10c) that ductile domal rises could also develop progressively during extension leading to rather late core complex-type structures. However, it must be pointed out that early core complexes (Figure 10d) are asymmetrical, like most of known natural examples, whereas late core complexes (Figure 10c) are symmetrical.

[34] So, even if we cannot exclude the development of late core complexes from localization effect within the brittle upper crust, the experimental results strongly suggest

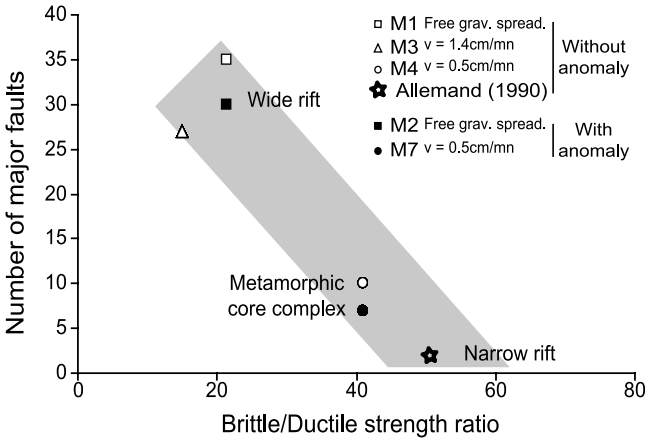

Figure 11. Comparison of wide rift and core complex modes of extension in terms of fault number and brittle-ductile strength ratio. The narrow rift position is determined from the experimental data of *Allemand* [1990]. Because in free gravity spreading experiments the velocity of displacement changes with time, the one taken here corresponds to the end of fault creation.

that core complex development is enhanced by extension rates lower than the potential rates of free gravity spreading and by the presence of heterogeneities within the ductile crust. Moreover, in a crust extending at a rate closer to those of potential free gravity spreading, core complexes can be considered as heterogeneities of stretching within wide rifts.

[35] In the Basin and Range and the Aegean, as already quoted (Basin and Range from *Coney* [1987] and Aegean from *Gautier et al.* [1999]), the development of metamorphic core complexes precedes wide rifting, an evolution that cannot be simulated by the analogue models. This is mostly due to the fact that analogue models are unable to take into account the variation of temperatures during extension and the consequent rheological changes. In an extending crust, thinning is accompanied by a progressive cooling and therefore by a downward migration of the brittle-ductile transition and a viscosity increase of the still ductile crust. This evolution progressively must change the coupling between brittle and ductile layers. However, the models that separately simulate metamorphic core complexes and wide rifts may be considered as two successive stages of evolution of an extending crust.

6.2. Dynamics of Faulting

[36] The comparison between free gravity and boundary controlled gravity spreading experiments shows that the dynamics of faulting in the upper brittle layer strongly depends on the velocity applied at model boundary. All models show that major faulting in the upper brittle layer develops at an early stage of extension, before 35% of stretching (Figure 9b). The duration of major faults creation, however, tends to increase when the velocity decreases.

[37] From the experiments, it appeared that the number of major faults is a direct function of strain rate and therefore also of ductile strength. The grey band in Figure 11 suggests that the number of major faults decreases almost linearly with increasing brittle-ductile strength ratio. The diagram also shows that modes of wide rift and core complexes that develop without anomaly likely represent end-member cases of the extensional process. However, if an anomaly is present, core complexes develop all along the trend. It is especially significant that core complex and narrow rift are located close to each other. This must be put in relation with the fact that the initial stage of core complexes corresponds to an upper crustal graben (Figure 8). In other terms, a core complex is a graben (or rift) whose deepening and widening is not accommodated by sedimentation but by ductile crust exhumation.

6.3. Asymmetry of Fault Patterns

[38] Free gravity spreading models (Figures 5 and 6) display asymmetrical fault patterns that likely result from the sense of shear along the brittle-ductile interface as argued by *Faugère and Brun* [1984] and *Brun et al.* [1994]. In model 1, the asymmetrical pattern results from a homogeneous deformation, in terms of bulk strain at model scale. A sense of shear top to the mobile wall, immediately below the brittle-ductile interface, is demonstrated in models with vertical markers in the ductile layer. Faults defining the tilted blocks in the brittle layer exhibit the same sense of shear. It is especially important to recall that except this top part of the ductile layer, sheared along the brittle-ductile interface, the rest of the ductile layer is deformed in pure shear mode. This comes from the fact that the ductile layer starts flowing slightly before faulting in the brittle layer. Consequently, even if most of the ductile layer is deforming in pure shear, the top part undergoes a layer-parallel shear against the base of the brittle layer. The state of stress, at the base of the brittle layer, is therefore modified, favoring the development of those potential normal faults whose sense of shear is compatible with the sense of shear imposed at the layer base.

[39] Model 2 is comparable to those previously described by *Brun et al.* [1994]. As a whole, the deformation appears laterally partitioned due to the presence of the dome. The most striking effect is the difference in thinning between the right and left sides of the dome that gives a strong asymmetry at model scale. The comparison with the previous model (Figure 5) shows that the presence of an anomaly within the ductile layer strongly modifies the mechanical behavior of the system. Whereas both models are asymmetrical, the fault patterns in the brittle layer are different, indicating opposite senses of shear on each side of the dome. Only the left-hand side of the model, close to the moving wall, displays a sense of shear comparable to the one of model 1.

6.4. Core Complex Development

[40] In the experiments, core complexes develop in two stages. Deformation starts with the development of a graben in the upper crust. The graben widening allows the rise and exhumation of a ductile layer dome (Figure 10d). This confirms the previous conclusion of *Brun et al.* [1994]

and is also illustrated in the numerical models of *Tirel et al.* [2004]. It is in agreement with the arguments of *Jolivet* [2001] and *Chéry* [2001], who suggested that the Gulf of Corinth graben could be the precursor of a future core complex.

[41] The models illustrate that a core complex results from a local necking of the brittle upper crust and further extreme thinning up to rupture level. From this point of view, one may consider that core complexes simply represent gaps between upper crust boudins, filled by material coming from the underlying ductile crust. This should be compatible with the concept of "crustal fluid layer" of *Wernicke* [1990, 1992]. Therefore, and contrary to the commonly accepted opinion, we consider the detachment not as the primary cause of the core complex development but as a consequence. This is at variance with the more classical conception of core complexes where the exhumation of ductile crust is explained as a consequence of the displacement along a so-called detachment fault that cross-cuts [*Wernicke*, 1985] or not [*Buck*, 1988; *Wernicke and Axen*, 1988] the entire crust.

[42] In our experimental models a detachment can be drawn on one limb of the ductile domal rise. The final attitude of this detachment is upward convex, flat on top of the dome and steeper on dome limb. Above the detachment, the hanging wall is asymmetrically faulted with small-scale tilted blocks. This fault pattern developed entirely within the early graben from faults that are steeply dipping at initiation, in agreement with the previous conclusions of *Brun et al.* [1994]. During exhumation of the ductile layer the detachment zone became parallel to the brittle-ductile transition, even if it not the case at the onset of extension. The experimental models are unable to describe the prolongation of the detachment zone within the underlying ductile layer. However, as shown by the numerical models of *Tirel et al.* [2004], the steeper part of the detachment joins at depth one of the flat lying shear zones that result from lower crustal flow associated to the domal rise.

[43] Core complex-type structures developing at an early stage of extension are obtained in the experiments when an anomaly of viscosity-density is placed below the brittle-ductile interface at once in free gravity spreading [see also *Brun et al.*, 1994] and boundary-controlled gravity spreading. The anomaly plays a major role in the localization of stretching. In free gravity spreading, it is only responsible for a local stronger amount of finite stretching that does not prevent extension and faulting to occur in the rest of the brittle layer. Moreover, in terms of faulting duration the anomaly does not play any significant role (Figure 9). On the contrary, in boundary-controlled gravity spreading the anomaly directly controls both the local amount of stretching and the duration of major faulting.

[44] The use of an anomaly of the ductile layer has been strongly criticized by *Koyi and Skelton* [2001], who preferred to use a fault-type preexisting discontinuity in the upper crust. In their analogue experiments, preexisting faults are cut with a 45° dip within a layer made of plasticine-based mixture. The strength of the layer is so high that almost no other fault developed during deformation and that the entire displacement remains localized within the precut anomaly. The implicit hypothesis of these models is that detachment faults result from the reactivation of preexisting faults. It is important to recall that it has never been demonstrated in the field that a detachment fault corresponds to the reactivation of a fault preexisting in the upper brittle crust. Moreover, at once in the Basin and Range and in the Aegean, core complexes do not develop everywhere in the extended domain but in rather localized zones. In the Aegean, they occur in only two areas, namely, the Cyclades and the southern Rhodope [see *Gautier et al.*, 1999], over an extended domain of about 1000 km. Considering the fact that preexisting faults cannot reasonably occur only in some particular zones of an orogenic domain and in addition to the previous arguments, it is doubtful that core complex development can be only controlled by preexisting faults.

[45] On the other hand, geological evidence pleads in favor of the rheological heterogeneity of the ductile crust. First of all, most of core complexes contain granites and migmatites and the detachment zones mylonites frequently involve synkinematic leucogranites (e.g., BR from *Davis and Coney* [1979], *Reynolds and Rehrig* [1980], and *Miller et al.* [1983] and Aegean from *Gautier et al.* [1993] and *Sokoutis et al.* [1993]). In fact, the evidence is so widespread that it has even been suggested that synkinematic granites can trigger the development of core complexes [*Lister and Baldwin*, 1993; *Parsons and Thompson*, 1993]. It is also important to recall that, on a broader scale, the development of core complexes is contemporaneous with magmatic activity (BR from *Davis and Coney* [1979], *Coney and Harms* [1984], and *Wernicke* [1992] and Aegean from *Jones et al.* [1992]). Consequently, it is not unreasonable to invoke the presence of rheological anomalies of the ductile crust.

[46] A diapiric effect of granites and migmatites has also been considered to play a role in the development of core complexes [e.g., *Norlander et al.*, 2002]. From the above considerations on the synchronism between magmatism and core complexes development, this possibility cannot be excluded. However, as differential stresses at the top of a rising granite diapir would be in the range of few bars or ten of bars [*Berner et al.*, 1972], far smaller than the strength of 10 to 20 km thick brittle crust. Therefore diapirism in itself should not be the primary cause of dome rise but buoyancy effects of granites and partially molten crust [*Gerya et al.*, 2001] can combine to extension in the growth of core complexes.

7. Conclusions

[47] The models presented here intend to simulate the extension of a thickened and thermally relaxed lithosphere in collisional domains, comparable to what occurred in the Basin and Range of western United States or in the Aegean. The initial conditions, in such "hot" lithospheres, allow a gravitational instability of spreading type at the scale of the brittle-ductile system. Two types of experiments were carried out to simulate free gravity spreading and boundary-

controlled gravity spreading, in order to compare their respective effects on the resulting extensional structures. Velocities applied in the experiments of boundary-controlled type were calibrated on velocities that were measured in free gravity spreading experiments. The range of model responses covers a large spectrum of deformation patterns relevant to wide rifts and core complexes. The most significant outcomes are the following.

[48] 1. Wide rift-type structures (i.e., block faulting at the scale of the whole system) develop spontaneously in models with a laterally homogeneous brittle-ductile layering. At the highest strain rates coupling between brittle and ductile layers is maximum leading to homogeneous tilted block patterns. For decreasing values of strain rates and brittle-ductile coupling faulting becomes more symmetrical, leading to horst and graben patterns. The modes of wide rift and core complexes that develop without anomaly likely represent end-member cases of the extensional process in terms of faulting dynamics and brittle-ductile strength ratio.

[49] 2. Core complex development is enhanced by extension rates lower than the potential rates of free gravity spreading. In a crust extending at a rate closer to those of potential free gravity spreading, core complexes can be considered as heterogeneities of stretching within wide rifts.

[50] 3. The presence of weak heterogeneities in the ductile layer favors the development of core complexes. In nature this could correspond to the presence of materials weaker than their environment, such as granite plutons of domains of partially molten rocks. At boundary velocities lower than those of free gravity spreading core complexes at an early stage of extension, directly comparable with what is observed in natural domains of large-scale extension (Basin and Range and Aegean).

[51] 4. Core complexes develop in two main stages. Deformation starts with a graben in the upper crust, which results from a necking instability of the brittle layer. The graben widening further allows the rise and exhumation of a ductile layer dome. A detachment progressively develops within the early graben from faults that are steeply dipping at initiation. During exhumation of the ductile layer, the detachment zone became progressively parallel to the brittle-ductile transition. The final geometry of the detachment is upward convex, flat on top of the dome and steeper on dome limb. In other terms and contrary to the commonly accepted opinion, the detachment is not the primary cause of the core complex development but a consequence.

Appendix A: Delineation of Fault Evolution During Progressive Deformation

[52] Because of lateral boundary effects, the evolution of faults in a vertical plane cannot be observed directly through lateral walls during deformation. The cross-sectional analysis of fault patterns can only be done at the end of experiments from model dissection. However, important information relative to progressive deformation can be obtained from photographs of model surface, taken at regular time intervals during experiments.

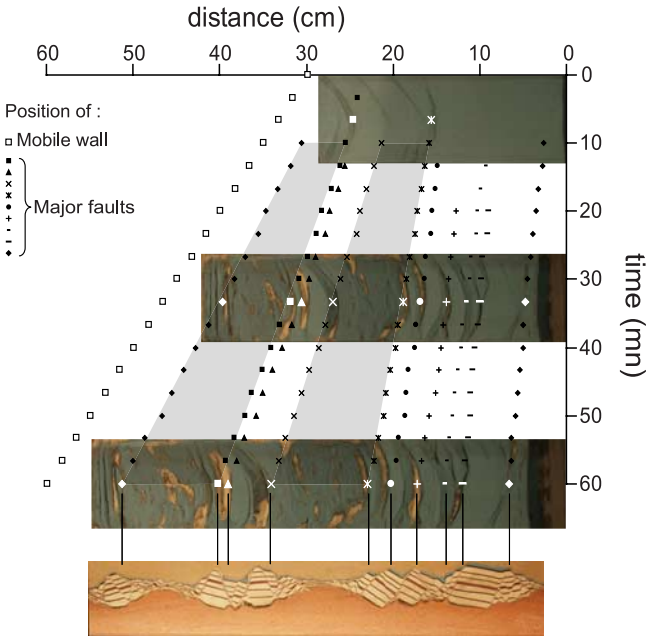

Figure A1. Diagram showing the progressive development of normal faults at model 4 (v = 0.5 cm min^{-1}) surface. Moderate fault curvature is due to lateral boundary shear. At each 200 s step, the position of all major faults is measured (10 different signs).

[53] For the purpose of the present study, the duration of major fault creation and the variation of fault positions during increasing stretching were especially important to consider. Figure A1 presents the principles of the method used to delineate the position of faults at model surface, here applied to model 4 (v = 0.5 cm min^{-1}, no anomaly in the ductile layer). The time interval between surface photographs is 200 s. On each photograph the position of all visible faults is located along the central axis of the model (see white signs on the three surface photographs in Figure A1).

[54] Processing model 4 in this way reveals that the two zones of extreme brittle crust thinning, i.e., local necking, observed in the final vertical cross section, have developed progressively and regularly during stretching. This is demonstrated by the divergence of position signs corresponding to faults bordering the necking zones (see grey bands in Figure A1).

[55] **Acknowledgments.** C. Tirel acknowledges her thesis grant from the French Ministry of Education and Research. This project was financially supported by the research funding attributed to J.-P. Brun by the Institut Universitaire de France. D. Sokoutis kindly acknowledges research grant by ISES (Netherlands Centre for Integrated Solid Earth Science) and NOW (Netherlands Organization for Scientific Research) for the financial support. C. Tirel thanks the group of experimental tectonics of the Vrije Universiteit for technical assistance and discussion in the laboratory, with special thanks to G. Corti and E. Willingshoffer for enlightening exchanges on modeling. The authors would also like to thank the Editor and Associate Editor Onno Onken and Lothar Ratsbacher, as well as the referees Claudio Faccenna and Nina Kukoski, for their suggestions of improvement. Further constructive comments by Claudio Faccenna were very welcome, especially concerning the relationship between the number of faults and the brittle-ductile strength ratio.

References

Allemand, P. (1990), *Approche Expérimentale de la Mécanique du Rifting Continental*, 205 pp., Univ. de Rennes 1, Rennes, France.

Allmendinger, R. W., K. Nelson, C. Potter, M. Barazangi, L. B. Brown, and J. E. Oliver (1987), Deep seismic reflection characteristics of the continental crust, *Geology*, *15*, 304–310.

Andersen, T. B., B. Jamtveit, J. F. Dewey, and E. Swensson (1991), Subduction and eduction of continental crust: Major mechanisms during continent-continent collision and orogenic extensional collapse, a model based on the South Norwegian Caledonides, *Terra Nova*, *3*, 303–310.

Berner, H., H. Ramberg, and O. Stephansson (1972), Diapirism in theory and experiment, *Tectonophysics*, *15*, 197–218.

Bird, P. (1979), Continental delamination and the Colorado Plateau, *J. Geophys. Res.*, *84*, 7561–7571.

Block, L., and L. H. Royden (1990), Core complex geometries and regional scale flow in the lower crust, *Tectonics*, *9*, 557–567.

Brun, J.-P. (1999), Narrow rifts versus wide rifts; inferences for the mechanics of rifting from laboratory experiments, *Philos. Trans. R. Soc. London, Ser.*, 695–712.

Brun, J.-P., D. Sokoutis, and J. Van Den Driessche (1994), Analogue modeling of detachment fault systems and core complexes, *Geology*, *22*, 319–322.

Buck, W. R. (1988), Flexural rotation of normal faults, *Tectonics*, *7*, 959–973.

Buck, W. R. (1991), Modes of continental lithospheric extension, *J. Geophys. Res.*, *96*, 20,161–20,178.

Burg, J. P., J. Van Den Driessche, and J.-P. Brun (1994), Syn to post-thickening extension in the Variscan Belt of western Europe: Modes and structural consequences, *Geol. Fr.*, *3*, 33–51.

Byerlee, J. D. (1978), Friction of rocks, *Pure Appl. Geophys.*, *116*, 615–626.

Chéry, J. (2001), Core complex mechanics: From the Gulf of Corinth to the Snake Range, *Geology*, *29*, 439–442.

Clark, M. K., and L. H. Royden (2000), Topographic ooze: Building the eastern margin of Tibet by lower crustal flow, *Geology*, *28*, 703–706.

Coney, P. J. (1987), The regional tectonic setting and possible causes of Cenozoic extension in the North American Cordillera, in *Continental Extensional Tectonics*, edited by M. P. Coward, J. F. Dewey and P. L. Hancock, *Geol. Soc. Spec. Publ.*, *28*, 177–186.

Coney, P. J., and T. A. Harms (1984), Cordilleran metamorphic core complexes: Cenozoic extensional relics of Mesozoic compression, *Geology*, *12*, 550–554.

Crittenden, M. D., P. J. Coney, and G. H. Davis (1980), Cordilleran metamorphic core complexes, *Mem. Geol. Soc. Am.*, *153*, 490 pp.

Davis, G. A., and P. J. Coney (1979), Geological development of metamorphic core complexes, *Geology*, *7*, 120–124.

Dewey, J. F. (1988), Extensional collapse of orogens, *Tectonics*, *7*, 1123–1139.

Doin, M. P., and L. Fleitout (1996), Thermal evolution of the oceanic lithosphere: An alternative view, *Earth Planet. Sci. Lett.*, *142*, 121–136.

England, P. C., and S. W. Richardson (1977), The influence of erosion upon the mineral facies of rocks from different metamorphic environments, *J. Geol. Soc. London*, *22*, 201–213.

England, P. C., and A. Thompson (1986), Some thermal and tectonic model for crustal melting in continental collision zones, in *Collision Tectonics*, edited by M. P. Cowards and A. C. Ries, *Geol. Soc. Spec. Publ.*, *19*, 83–94.

Faugère, E., and J.-P. Brun (1984), Modélisation expérimentale de la distension continentale, *C. R. Acad. Sci.*, *299*, 365–370.

Gaudemer, Y., C. Jaupart, and P. Tapponnier (1988), Thermal control on post-orogenic extension in collision belts, *Earth Planet. Sci. Lett.*, *89*, 48–62.

Gautier, P., J.-P. Brun, and L. Jolivet (1993), Structure and kinematics of Upper Cenozoic extensional detachment on Naxos and Paros (Cyclades Islands, Greece), *Tectonics*, *12*, 1180–1194.

Gautier, P., J. P. Brun, R. Moriceau, D. Sokoutis, J. Martinod, and L. Jolivet (1999), Timing, kinematics and cause of Aegean extension: A scenario based on a comparison with simple analogue experiments, *Tectonophysics*, *315*, 31–72.

Gerya, T. V., W. V. Maresch, A. P. Willner, D. D. Van Reenen, and C. A. Smit (2001), Inherent gravitational instability of thickened continental crust regionally developed low- to medium-pressure granulite facies metamorphism, *Earth Planet. Sci. Lett.*, *190*, 221–235.

Hauser, E., C. Potter, T. Hauge, S. Burgess, S. Burtch, J. Murtschler, R. Allmendinger, L. Brown, S. Kaufman, and J. Oliver (1987), Crustal structure of eastern Nevada from COCORP deep seismic reflection data, *Geol. Soc. Am. Bull.*, *99*, 833–844.

Hubbert, K. (1937), Theory of scale models as applied to the study of geological structures, *Geol. Soc. Am. Bull.*, *48*, 1459–1520.

Jolivet, L. (2001), A comparison of geodetic and finite strain in the Aegean, geodynamic implications, *Earth Planet. Sci. Lett.*, *187*, 95–104.

Jones, C. E., J. Tarney, J. H. Baker, and F. Gerouki (1992), Tertiary granitoids of Rhodope, northern Greece: Magmatism related to extensional collapse of the Hellenic Orogen?, *Tectonophysics*, *210*, 295–314.

Koyi, H. A., and A. Skelton (2001), Centrifuge modelling of the evolution of low-angle detachment faults from high-angle normal faults, *J. Struct. Geol.*, *23*, 1179–1185.

Le Pichon, X. (1982), Land-locked oceanic basins and continental collision: The Eastern Mediterranean as a case example, in *Mountain Building Processes*, edited by K. J. Hsü, pp. 201–211, Elsevier, New York.

Lister, G. S., and S. L. Baldwin (1993), Plutonism and the origin of metamorphic core complexes, *Geology*, *21*, 607–610.

Makris, J., and R. Vees (1977), Crustal structure of the central Aegean Sea and the islands of Evia and Crete, Greece, obtained by refractional seismic experiments, *J. Geophys.*, *42*, 329–341.

McClusky, S., et al. (2000), Global Positioning System constraints on plate kinematics and dynamics in the eastern Mediterranean and Caucasus, *J. Geophys. Res.*, *105*, 5695–5719.

McKenzie, D. (1978), Active tectonics of the Alpine-Himalayan belt: The Aegean Sea and surrounding regions, *Geophys. J. R. Astron. Soc.*, *55*, 217–254.

McKenzie, D., and J. Jackson (2002), Conditions for flow in the continental crust, *Tectonics*, *21*(6), 1055, doi:10.1029/2002TC001394.

Mercier, J. L. (1981), Extensional-compressional tectonics associated with the Aegean Arc: Comparison with the Andean Cordillera of south Peru-north Bolivia, *Philos. Trans. R. Soc. London, Ser. A*, *300*, 337–355.

Miller, E. L., P. B. Gans, and J. Garing (1983), The Snake Range décollement: An exhumed mid-Tertiary ductile-brittle transition, *Tectonics*, *2*, 239–263.

Nalpas, T., and J.-P. Brun (1993), Salt flow and diapirism related to extension at crustal scale, *Tectonophysics*, *228*, 349–362.

Norlander, B. H., D. L. Whitney, C. Teyssier, and O. Vanderhaeghe (2002), Partial melting and decompression of the Thor-Odin dome, Shuswap metamorphic core complex, Canadian Cordillera, *Lithos*, *61*, 103–125.

Oxburg, E. R., and D. Turcotte (1974), Thermal gradients and regional metamorphism in overthrust terrains with special reference to eastern Alps, *Schweiz. Mineral. Petrogr. Mitt.*, *54*, 641–662.

Parsons, T., and G. A. Thompson (1993), Does magmatism influence low-angle normal faulting?, *Geology*, *21*, 247–250.

Ramberg, H. (1981), *Gravity, Deformation and Earth's Crust*, 2nd ed., 452 pp., Elsevier, New York.

Ranalli, G. (1997), Rheology of the lithosphere in space and time, in *Orogeny Through Time*, edited by J. P. Burg and M. Ford, *Geol. Soc. Spec. Publ.*, *121*, 19–37.

Rey, P., O. Vanderhaeghe, and C. Teyssier (2001), Gravitational collapse of the continental crust: Definition, regimes and modes, *Tectonophysics*, *342*, 435–449.

Reynolds, S. J., and W. A. Rehrig (1980), Mid-Tertiary plutonism and mylonitization, South Mountains, central Arizona, in *Cordilleran Metamorphic Core Complexes*, edited by M. C. Crittenden, P. J. Coney, and G. H. Davis, *Mem. Geol. Soc. Am.*, *153*, 159–175.

Royden, L. (1996), Coupling and decoupling of crust and mantle in convergent orogens: Implications for strain partitioning in the crust, *J. Geophys. Res.*, *101*, 17,679–17,705.

Smith, R. B., and G. P. Eaton (1978), *Cenozoic Tectonics and Regional Geophysics of the Western Cordillera*, *Mem. Geol. Soc. Am.*, *152*, 388 pp.

Sokoutis, D., J. P. Brun, J. Van Den Driessche, and S. Pavlides (1993), A major Oligo-Miocene detachment in southern Rhodope controlling north Aegean extension, *J. Geol. Soc. London*, *150*, 243–246.

Sonder, L. J., P. C. England, B. P. Wernicke, and R. L. Christiansen (1987), A physical model for Cenozoic extension of western North America, in *Continental Extensional Tectonics*, edited by M. P. Coward, J. F. Dewey, and P. L. Hancock, *Geol. Soc. Spec. Publ.*, *28*, 187–201.

Stewart, J. H. (1978), Basin-range structure in western North America: A review, in *Cenozoic Tectonics and Regional Geophysics of the Western Cordillera*, edited by R. B. Smith and G. P. Eaton, *Mem. Geol. Soc. Am.*, *152*, 1–31.

Tirel, C., J.-P. Brun, and E. Burov (2004), Thermomechanical modeling of extensional gneiss domes, in *Gneiss Domes in Orogeny*, edited by D. L. Whitney, C. Teyssier, and C. S. Siddoway, *Spec. Pap. Geol. Soc. Am.*, *380*, 67–78.

Vendeville, B., P. R. Cobbold, P. Davy, J.-P. Brun, and P. Choukroune (1987), Physical models of extensional tectonics at various scales, in *Continental Extensional Tectonics*, edited by M. P. Coward, J. F. Dewey, and P. L. Hancock, *Geol. Soc. Spec. Publ.*, *28*, 95–107.

Wernicke, B. (1981), Low-anle normal faults in the Basin and Range Province: Nappe tectonics in an extending orogen, *Nature*, *291*, 645–648.

Wernicke, B. (1985), Uniform-sense normal simple shear of the continental lithosphere, *Can. J. Earth Sci.*, *22*, 108–125.

Wernicke, B. (1990), The fluid crustal layer and its implications for continental dynamics, in *Exposed Cross-Sections of the Continental Crust*, edited by M. H. Salisbury and D. M. Fountain, pp. 509–544, Springer, New York.

Wernicke, B. (1992), Cenozoic extensional tectonics of the U.S. Cordillera, in *The Geology of North America*, vol. G-3, *The Cordilleran Orogen: Conterminous U.S.*, edited by B. C. Burchfield, P. W. Lipman, and M. L. Zoback, pp. 553–581, Geol. Soc. of Am., Boulder, Colo.

Wernicke, B., and G. J. Axen (1988), On the role of isostasy in the evolution of normal fault systems, *Geology*, *16*, 848–851.

J.-P. Brun, Géosciences Rennes, Université de Rennes1, UMR 6118, F-35042, Rennes, France.

D. Sokoutis, Netherlands Centre for Integrated Solid Earth Science, Faculty of Earth and Life Sciences, De Boelelaan 1085, Vrije Universiteit, NL-1081 HV Amsterdam, Netherlands.

C. Tirel, Faculty of Geosciences, Tectonophysics, Vrije Universiteit, Budapestlaan 4, NL-3584, CD Utrecht, Netherlands. (tirel@geo.uu.nl)